Journal of Applied Physics

Fourier plane imaging microscopy

Cite as: J. Appl. Phys. **116**, 103102 (2014); https://doi.org/10.1063/1.4895157
Submitted: 18 May 2014 . Accepted: 29 August 2014 . Published Online: 09 September 2014

Daniel Dominguez, Nouf Alharbi, Mdhaoui Alhusain, Ayrton A. Bernussi, and Luis Grave de Peralta

JOURNAL OF APPLIED PHYSICS **116**, 103102 (2014)

Fourier plane imaging microscopy

Daniel Dominguez,[1,2,a)] Nouf Alharbi,[1] Mdhaoui Alhusain,[1] Ayrton A. Bernussi,[2,3] and Luis Grave de Peralta[1,2]
[1]*Department of Physics, Texas Tech University, Lubbock, Texas 79409, USA*
[2]*Nano Tech Center, Texas Tech University, Lubbock, Texas 79409, USA*
[3]*Department of Electrical and Computer Engineering, Texas Tech University, Lubbock, Texas 79409, USA*

(Received 18 May 2014; accepted 29 August 2014; published online 9 September 2014)

We show how the image of an unresolved photonic crystal can be reconstructed using a single Fourier plane (FP) image obtained with a second camera that was added to a traditional compound microscope. We discuss how Fourier plane imaging microscopy is an application of a remarkable property of the obtained FP images: they contain more information about the photonic crystals than the images recorded by the camera commonly placed at the real plane of the microscope. We argue that the experimental results support the hypothesis that surface waves, contributing to enhanced resolution abilities, were optically excited in the studied photonic crystals. © *2014 AIP Publishing LLC*.
[http://dx.doi.org/10.1063/1.4895157]

I. INTRODUCTION

Imaging is by far one of the most basic assessments in many scientific investigations. The compound optical microscope remains one of the most versatile and widely used optical instruments in the lab.[1] A typical compound microscope includes an objective lens and an eyepiece formed by a second set of lenses.[2–4] In modern compound microscopes, a camera placed at the microscope's real plane (RP) collects the image of the object under observation; then, after some digital processing, the RP image is displayed on a computer screen. The compound microscope has been used in numerous far-field optical microscopy techniques with a variety of configurations, illumination sources, and cameras. It is contactless, simple to use, may not require special sample fabrication, the samples can be imaged under different environmental conditions, and it is usually cost-effective. As a result, the almost inexorable presence of the compound microscope in optical laboratories continues to motivate further instrument development. Many advances have been made in designing easy-to-use optical components that produce high-resolution images.[1] In particular, the optical condenser, which consists of a combination of bulky lenses (or mirrors) and diaphragms designed to illuminate the sample with a cone of inclined light, has been largely used as a simple optical element to improve image resolution.[5] When a coherent beam of light impinges normally on the sample in a traditional compound microscope, the minimum observable period is $p_{min} \sim \lambda/NA_o$,[2–4] where λ is the wavelength of the illumination source in vacuum, and NA_o is the numerical aperture of the microscope objective lens. Illuminating the sample with very wide angles, provided by a condenser, improves the microscope resolution and reduces p_{min} to $\sim\lambda/(2NA_o)$,[6–9] which is the well-known Rayleigh resolution limit of diffraction-limited imaging instruments.[2–9] Ultrathin condensers (UTC), occupying a volume three orders of magnitude smaller than bulky condensers[9] and digital condensers with no lenses, mirrors, or moving parts,[10–12] have been recently reported. Moreover, the use of a compound microscope with a planar digital condenser to obtain reconstructed images with resolution several times smaller than the Rayleigh resolution limit has been recently demonstrated.[11]

In this work, we describe the application of a Fourier plane based microscopy imaging technique used in conjunction with a compound microscope to image photonic crystals (PC).[9,13] In our experiments, we used the microscope's built-in illumination source, which emits a beam of white light perpendicular to the sample. We added a second camera to the microscope to capture the Fourier plane (FP) image formed in the back focal plane of the microscope's objective lens. As expected, when the period (p) of the photonic crystal was larger than λ/NA_o, the photonic crystal's structures were observed by the RP camera. In contrast, we show that when $p < \lambda/NA_o$, the images in the RP camera cannot resolve the photonic crystal structure; yet, we demonstrate that the image of the photonic crystals can always be recovered using the corresponding FP image obtained from the second camera (or FP camera). This is possible due to a remarkable property of the FP images captured by the FP camera: they contain more information about the photonic crystal that can be obtained by the images captured by the RP camera. It is worth noting that the amount of information arriving to the microscope's FP is equal to the amount of information arriving to the microscope's RP. However, the type of information recorded in the FP (RP) image is not equal to the information arriving to the microscope's FP (RP). We show here that there is more information about the PC in the recorded information in the FP image than in the recorded information in the RP image. We term this microscopy technique FP Imaging Microscopy (FPIM) because the imaging method requires only the capture of a single FP image. In the experiments described here, no bulky microscope condensers were used; however, we show that our unexpected experimental results can be explained using the image formation theory developed for microscopes based on the use of UTCs.[14] FPIM resembles traditional, lensless, X-ray

a)Electronic mail: daniel.dominguez@ttu.edu

diffraction crystallography, where the periodic structure of a crystal is determined from the recorded diffraction pattern.[15] However, the use of an objective lens in FPIM allows for better control of the optical environment and light collection with large numerical aperture. Concerning the resemblance between FPIM and diffractometry, we discuss how adding a FP camera to a compound microscope transforms the instrument into a low-resolution but useful spectrometer and a far field, non-scanning, Fourier plane imaging microscope.

This paper is organized as follows: In Sec. II, we describe the experimental arrangement and the procedure used to image photonic crystals. Section III is dedicated to the discussion of the results obtained with an unexpected condenser. In Sec. IV, we discuss the FPIM technique used to image photonic crystals, whose periods are below that allowed by the microscope's resolution limit for normal incidence illumination. Section V describes experiments, where the combination of a compound microscope with the unexpected condenser is used as a spectrometer. Finally, the conclusions of this work are given in Sec. VI.

II. EXPERIMENTAL ARRANGEMENT AND PRELIMINARY RESULTS

Figure 1 shows schematic illustrations of the microscope arrangement and the structure of the photonic crystal samples used in our experiments. The experimental arrangement used, shown schematically in Fig. 1(a), consisted of a Nikon Eclipse Ti inverted microscope with a high numerical aperture ($NA_o > 1$) 100× magnification oil-immersion objective lens that was fitted with charge-coupled device (CCD) cameras to obtain the RP and FP images. The microscope's built-in source provided white light illumination at normal incidence. A $\lambda = 570$ nm centered wavelength band-pass filter with a bandwidth of $\Delta\lambda = 10$ nm was placed after the objective lens to select only a small spectral region from the illumination source. The PCs, shown in Fig. 1(b), were fabricated as follows: first, a ∼110 nm layer of PMMA-A4, serving as the patterning resist for e-beam lithography, was spin coated on top of a ∼150 μm glass cover slip. A ∼10 nm layer of aluminum was thermally deposited on top of the PMMA layer to provide a conductive grounding surface for the e-beam lithography patterning process. After the lithography step, the aluminum layer was etched off using hydrofluoric acid, and the PMMA was developed using a Methyl-isobutyl-keytone:Isopranol (MIBK:IPA) 1:3 solution. The holes remaining in the PMMA layer were patterned in a square or hexagonal lattice arrangement with different periods. To make the sample shown in Fig. 1(c), a 15 nm layer of chromium was deposited on top of the patterned PMMA layer using e-beam evaporation. The sample was then immersed in acetone to lift-off the PMMA layer thereby revealing the chromium segments that adhered to the glass substrate as pillars in a square lattice arrangement.

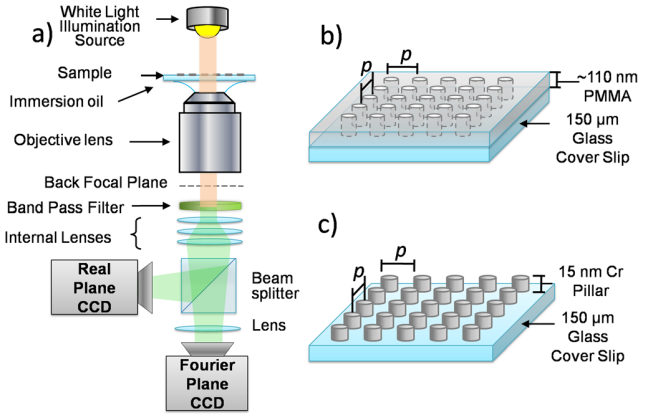

FIG. 1. (a) Microscope arrangement showing the components contributing to our results. (b) and (c) Schematic illustrations of the photonic crystals comprised of (b) air holes in a PMMA layer, and (c) chromium pillars on a glass substrate arranged in a square lattice.

The RP and FP images of PC formed by holes in a PMMA layer (Fig. 1(b)), obtained with a $NA_o = 1.3$ objective lens, are shown in Fig. 2. The PC periods (p) were 500 nm, 450 nm, and 300 nm. The RP images shown in Figs. 2(b) and 2(d) reveal that the photonic crystal's square lattice with $p = 500$ nm and $p = 450$ nm, respectively, are clearly visible, but the RP images of the square and hexagonal lattices with $p = 300$ nm shown in Figs. 2(f) and 2(h), respectively, do not reveal the lattice structure. The corresponding FP images show circular spots associated with the diffraction of the normally incident light emitted by the microscopes illumination source, as well as portions of rings centered on the spots. The distribution of the portion of rings observed in the FP images shown in Figs. 2(e) and 2(g) clearly corresponds to the square and hexagonal symmetry, respectively, of the PC. In Figs. 2(a) and 2(c), the zero-order (centered) and the first-

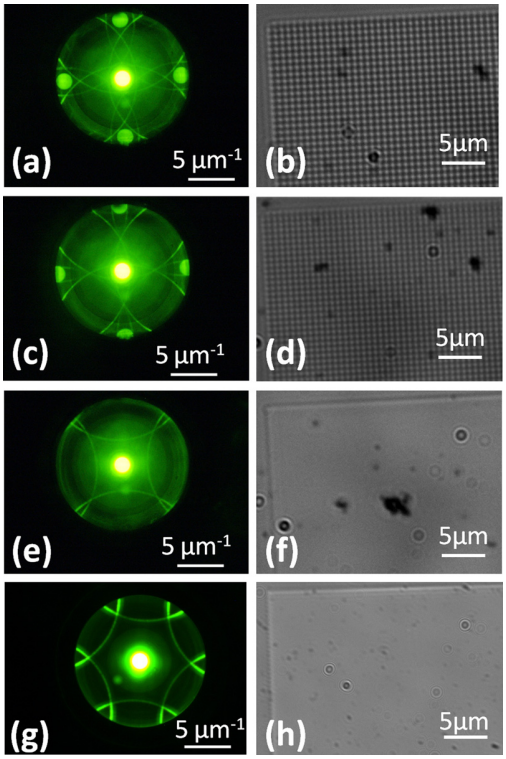

FIG. 2. Microscope (a), (c), (e), and (g) FP and (b), (d), (f), and (h) RP images of photonic crystals formed by holes in a PMMA layer with (a)–(f) square and (g) and (h) hexagonal symmetry. The period of the photonic crystal is (a) and (b) $p = 500$ nm, (c) and (d) $p = 450$ nm, and (e)–(h) $p = 300$ nm.

order (displaced from the center) diffraction spots are visible, but Figs. 2(e) and 2(g) show only the zero-order diffraction spot. All of these features in the FP images exist within a dim disk, whose boundary is the numerical aperture of the objective lens used. The FP images shown in Fig. 2 agree well with the Abbe's theory of image formation,[7,8] which states that structures in the RP image can only be resolved if the first-order diffraction spots are visible in the FP image. In good correspondence with Abbe's theory, our results revealed that the RP images corresponding to the FP images in Figs. 2(a) and 2(c) exhibited clearly resolved periodic structures since the first-order diffraction spots are visible in the FP images. In contrast, the RP images corresponding to the FP images in Figs. 2(e) and 2(g) do not reveal the PC structures. Our results also agree with the microscope's resolution limit for microscopes using normal incidence illumination, which defines the smallest period resolvable as $\lambda/NA_o \sim 570\,\text{nm}/1.3 \sim 440\,\text{nm}$.

III. AN UNEXPECTED MISCROSCOPE CONDENSER

An outstanding feature of the FP images in Fig. 2 is the set of (portions of) rings, whose origins have yet to be elucidated, but seem to be related with the light scattered by the circular aperture of the objective lens' metal cage. We established this relationship by illuminating the sample perpendicularly using a laser aimed through the pinhole opening of an iris diaphragm (to control the illumination spot size) instead of the microscope's built-in illumination source. We noted that the rings do not appear when the diameter of the laser beam is smaller than the aperture of the objective lens' metal cage, and the laser beam impinging the sample does not hit the metal cage of the microscope objective. It is clear that these rings are not a microscope artifact since their positions in the FP images depend on the period and symmetry of the analyzed structure and the rings move in synchrony with the first-order diffraction spots. FP images of a PC with $p = 600\,\text{nm}$ were obtained with the perpendicular illumination source (Fig. 3(a)) and with a traditional bulky condenser having numerical aperture $NA_c = 0.28$ (Fig. 3(b)) to show

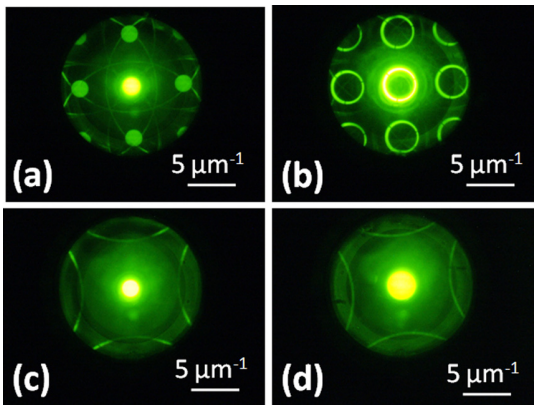

FIG. 3. (a) and (b) FP images of a photonic crystal formed by holes in a PMMA layer with period $p = 600\,\text{nm}$ illuminated with (a) the microscopes built-in perpendicular illumination source, and (b) traditional bulky condenser. (c) and (d) FP images of a photonic crystal with period $p = 250\,\text{nm}$ consisting of (c) holes in a PMMA layer, and (d) chromium pillars on glass.

how the spots, the condenser rings, and the rings all exhibit similar traits when a PC is present. The appearance of the rings is also independent of the type of photonic crystal used. Two PCs with structures similar to those illustrated in Figs. 1(b) and 1(c) were fabricated with identical periods $p = 250\,\text{nm}$. The FP image of the PC composed of air holes in a PMMA layer is shown in Fig. 3(c), and the FP image of the PC composed of chromium pillars on glass is shown in Fig. 3(d). The fact that the additional features observed are rings and that their positions in the FP change with different periods, similar to the rings observed when using plasmonic and non-plasmonic UTCs[9] as well as traditional condensers, suggests that the rings observed in our experiments might be the signature of an unpredicted new condenser.

The presence of a condenser in our microscopy arrangement should result in increased resolution; however, the RP images in Figs. 2(f) and 2(h) do not display any instances of increased resolution despite having visible portions of the first-order rings in the FP images shown in Figs. 2(e) and 2(g), respectively. The apparent discrepancy between our results and those expected from an analysis of Abbe's theory of image formation when a condenser is present is remedied by considering how images in the RP are produced from the FP features. In analogy with expected UTC behavior, in order to observe a periodic structure in the RP, features corresponding to at least two diffraction orders must be observed in the FP.[16] The diffraction features related with the unexpected condenser are the rings centered on the spots corresponding to perpendicular illumination; as such, portions of (or entire) rings corresponding to two diffraction orders must be captured. By analyzing the FP images presented in Figure 2, we can calculate the effective refractive index corresponding to the rings[17] to verify if the zero-order diffraction ring could be captured by the objective lens. The effective refractive index n_{eff} is calculated by taking the ratio of the diameter of the diffraction ring r_{ring} and the diameter of the dim lit disk r_{max}, and multiplying by the value of the numerical aperture of the objective, detailed in Fig. 4(a): $n_{eff} = NA_o \cdot r_{SPP}/r_{max}$.[17] Not surprisingly, the rings have an effective refractive index value of $n_{eff} = 1.4 > NA_o = 1.3$, which indicates as it is illustrated in Figure 4(a) that the zero-order diffraction ring exists outside of the objective lens' numerical aperture and cannot be collected. In summary, the RP images shown in Figures 2(b) and 2(d) have clearly visible periodic structures since both the zero- and first-order diffraction spots corresponding to perpendicular illumination are visible; while the RP images in Figs. 2(f) and 2(h) show no periodic features since they only exhibit the zero-order diffraction *spot* and portions of the first-order diffraction *rings* (no first-order diffraction spot nor zero-order diffraction rings).

An objective lens with a numerical aperture $NA_o > n_{eff}$ should capture both the zero- and first-order diffraction rings thereby revealing an image of the PC. This can be verified by the FP and RP images shown in Figures 4(b) and 4(c), respectively. These images correspond to a PC comprised of chromium pillars arranged with period $p = 300\,\text{nm}$, and were obtained using an objective lens with $NA_o = 1.49 > n_{eff}$ and by implementing a spatial filter to block the center spot,

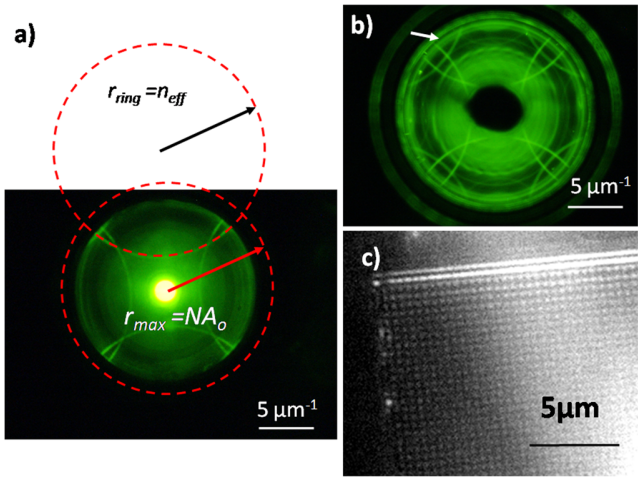

FIG. 4. (a) FP image shown in Fig. 2(e) with the first-order ring generated from an arc segment within NA_o and the parameters used to calculate n_{eff}. (b) FP image, with center spot spatial filtered, of a chromium/glass photonic crystal with period $p = 300$ nm. The arrow points at the dark zero-order diffraction ring. (c) Corresponding RP image of the same $p = 300$ nm photonic crystal showing the photonic crystal structure.

corresponding to the perpendicular illumination source, which enhanced the image contrast. The increased resolution is decisive evidence that the observed rings do indeed exhibit behavior typical of a condenser having a numerical aperture $NA_c \equiv n_{eff}$. It is worth noting that the RP image shown in Fig. 4(c) is formed only by light collected from the observed rings since no diffraction spots corresponding to perpendicular illumination are visible in the FP image shown in Fig. 4(b). Moreover, the RP image shown in Fig. 4(c) looks like a typical image obtained using a dark field microscopy technique. This is because, in contrast with the bright first-order diffraction rings observed in the FP image shown in Fig. 4(b), the zero-order diffraction ring (indicated by the arrow in Fig. 4(b)) is dark. A comparison of these experimental findings with similar results obtained using UTC[9,14] suggests that the rings observed in the experiments described here correspond to leakage radiation coupled to evanescent waves excited in the surface of the PCs by scattering of the perpendicular illumination. While the origin of these rings have yet to be completely determined, we can analyze the expected resolution increase from the rings associated with this unexpected condenser by calculating the resolution limit of a compound microscope with a condenser, given by the following expression:[7,9,12]

$$p_{\min} = \frac{\lambda}{NA_o + NA_c}, \tag{1}$$

where $NA_c = n_{eff}$. Using this expression and the values $\lambda = 570$ nm, $NA_c = 1.4$, and $NA_o = 1.49$, we determined $p_{min} = 197$ nm, which indicates that we should be able to image PCs with periods well below $p = 300$ nm. It is worth emphasizing that, as it shown in the RP images in Figs. 2(f) and 2(h), this expression is not valid when $NA_c > NA_o$. The results shown in Figs. 2 and 3 reveal that observation of the photonic crystal's periodic structure in the RP image is dependent on the observation of the zero-order diffraction ring in the FP image. In other words, it is compulsory that for compound microscopes that utilize condensers since they are diffraction limited when $NA_c = NA_o$.

IV. FOURIER PLANE IMAGING MICROSCOPY

In the experiments, where small numerical aperture objectives are used and $NA_c > NA_o$, images of PCs with periods smaller than the microscope's resolution limit under perpendicular illumination can be obtained by using the FPIM method as follows. The FP image shown in Fig. 3(c), obtained using a $NA_o = 1.3$ objective lens and perpendicular illumination, corresponds to a PC consisting of air holes in a PMMA layer with period $p = 250$ nm. The resolution limit for a compound microscope with perpendicular, $\lambda = 570$ nm, illuminating light is $p_{min} \sim \lambda/NA_o = 438$ nm. It is clear from this calculation, and from the missing first-order diffraction spots in the FP image shown in Fig. 3(c) that the photonic crystal's structure cannot be resolved in the RP. Moreover, although the first-order diffraction rings are present in the FP image shown in Fig. 3(c), the zero-order diffraction ring was not captured since $NA_c > NA_o$, and the condenser-related rings will therefore be unable to provide any resolution enhancements. Nonetheless, the arcs visible within the numerical aperture in the FP image allows us to reconstruct the full rings corresponding to the zero- and first-order diffraction rings, and from them we can determine the locations of the diffraction spots corresponding to perpendicular illumination. Figure 5(a) shows the reconstructed rings (dashed red lines), their respective centers (red dots), and the synthetic numerical aperture NA_s (solid line), which is drawn to encompass the first-order spots. Figure 5(b) shows a simpler version of a synthetic FP image formed by the periodic array

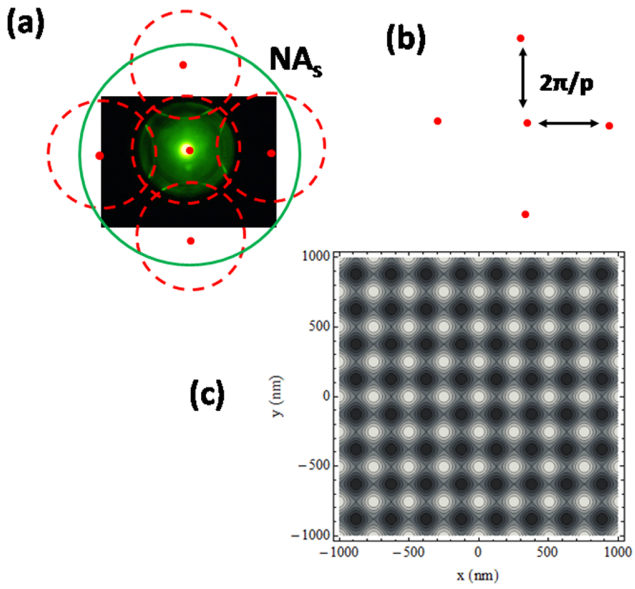

FIG. 5. (a) FP image of the photonic crystal formed by holes in a PMMA layer with $p = 250$ nm with the zero- and first-order rings generated from the arcs present within NA_o (dashed lines), the ring's respective centers (spots), and the synthetic numerical aperture NA_s (solid line). (b) An image of the spots used in the FPIM technique to calculate the reciprocal space period Λ. (c) The reconstructed RP image of the photonic crystal from the synthetic FP image.

of spots with a period $\Lambda = 2\pi/p$ (Refs. 14–17) determined from the features used to build the synthetic FP image in Fig. 5(a). The spots visible in the simplified synthetic FP image would be formed in the FP camera of the compound microscope if $NA_o \geq NA_s$. In a first approximation, the five narrow bright spots forming the simplified synthetic FP image shown in Fig. 5(b) could be described by the optical disturbance at the back focal plane of the microscope's objective lens as follows:[4,14]

$$U_{FP,s}(k_x,k_y) \propto \left[4\delta(k_x,k_y) + \delta\left(k_x - \frac{2\pi}{p}, k_y\right) + \delta\left(k_x + \frac{2\pi}{p}, k_y\right) + \delta\left(k_x, k_y - \frac{2\pi}{p}\right) + \delta\left(k_x, k_y + \frac{2\pi}{p}\right)\right], \quad (2)$$

where δ is the Dirac delta function,[4] and we have assumed, for convenience, that the amplitude corresponding to the zero-order diffraction spot is four times more intense than the amplitude corresponding to the first-order diffraction spots. The intensity distribution in the synthetic RP image, $I_{RP,s}(x,y)$, is then proportional to the absolute value of the Fourier transform of $U_{FP}(k_x,k_y)$;[4] therefore

$$I_{RP,s}(x,y) \propto \left[2 + \cos\left(\frac{2\pi}{p}x\right) + \cos\left(\frac{2\pi}{p}y\right)\right]. \quad (3)$$

For our PC, we calculated a reciprocal space separation between spot locations determined by the synthetic FP image of $\Lambda = 24.951\,\mu\text{m}^{-1}$, which corresponds to a period $p = 251.8\,\text{nm}$. Using expression (3), and the calculated PC period, a RP image of the two-dimensional periodic PC was reconstructed, shown in Fig. 5(c). The RP image of the PC formed by Cr pillars with a nominal $p = 250\,\text{nm}$ can be reconstructed in a similar way due to the similitude between the FP images shown in Figs. 3(c) and 3(d). The reconstruction of the RP image of the PC with hexagonal symmetry, whose FP image is shown in Fig. 2(g), can be done in a similar way; however, this time numerically calculating the Fourier transform of the synthetic FP image.

Our ability to reconstruct RP images from FP images unequivocally demonstrates that the FP images contain more information about the PC than the RP images, and that the FPIM method is capable of extracting it via FP image synthesis. This is possible because, when $p < \lambda/NA$ and $NA_c > NA_o$, there is an important difference in the type of information about the PC captured by the camera at each microscope plane. In the Abbe's theory of image formation in a microscope,[2–4,7,8] the RP image is formed by interference of light passing through diffraction features of different orders. However, as it is shown in the FP images shown in Figs. 2(e) and 2(g), only first order diffraction features are collected by the microscope objective when $p < \lambda/NA$ and $NA_c > NA_o$. As a consequence, no interference of light passing through diffraction features of different orders occurs and, as it is shown in Figs. 2(f) and 2(h), all the information about the PC structure is lost in the RP image. However, the FP image is formed by interference of light coming from the object following different optical paths. This is why the first order interference maxima carry information about the structure of the object. This information is contained in the arcs observed in the FP images. The Fourier transform of the homogeneous light distribution observed in the RP images shown in Figs. 2(f) and 2(h) is just a spot. The rings observed in the FP images shown in Figs. 2(e) and 2(g) cannot be recovered by numerical post-processing from the corresponding RP images. Based on our hypothesis about the origin of the observed rings, i.e., that the rings are produced by leaked light coupled to evanescent waves, we can describe the experimental results presented here using a previously developed theory of image formation in a microscope using UTCs.[9,14] The details about how the surface waves are excited are still unclear at this point, but we assume that evanescent waves are excited at the glass/air interface of the sample when the light emitted by the microscope illumination source is scattered by the circular aperture of the objective lens' metal cage. Following the theory of image formation developed in Ref. 14, we assume that (1) surface waves are excited in all directions, (2) each surface wave coherently illuminates the object under observation, (3) surface waves propagating in different directions are not coherent with each other, and (4) the excited waves leak to the glass coverslip. The leaked light collected by the microscope objective lens is the light used for imaging; therefore, the observed FP and RP images are formed due to the incoherent superposition of the intensity distributions at the microscope's FP and RP corresponding to the leaked light coupled

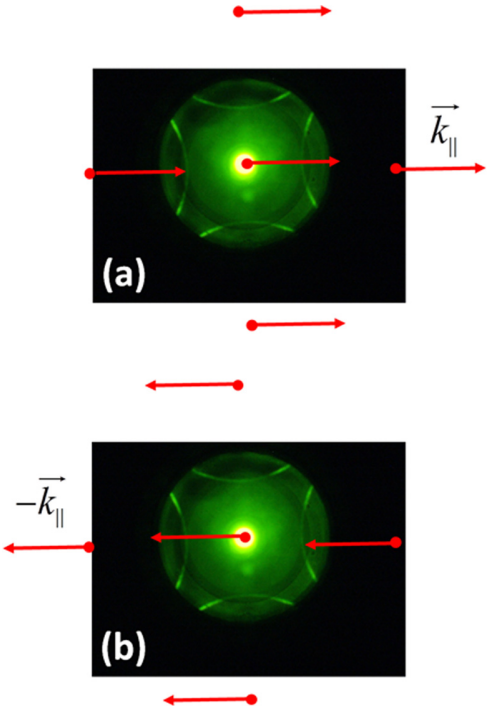

FIG. 6. Schematic illustration of the formation of the FP image shown in Fig. 3(c). The extreme of the five arrows point to the shifted diffraction spots that would be produced by the plasmonic crystal if the light would leak only in the direction determinate by the vectors (a) $\vec{k}_{\|}$ and (b) $-\vec{k}_{\|}$. The only one of the five arrows extremes, which is inside of the objective lens numerical aperture, contributes to the formation of the observed portion of rings.

to evanescent waves propagating in all directions.[14] Fig. 6 illustrates how the FP image shown in Figs. 3(c) and 5(a) was formed by the incoherent superposition of diffraction patterns corresponding to different illumination directions. The red spots correspond to the diffraction pattern that would be produced by the photonic crystal under out-of-plane perpendicular illumination. The arrows in Figs. 6(a) and 6(b) represent two instances of the parallel-to-the-surface component of the leaking light wave-vectors corresponding to two opposite directions of propagation of the excited surface waves, where $k_{\|} = (2\pi/\lambda)n_{eff}sen(\theta)$ and θ is the leaking angle.[14] The five extremes of the vectors in Figs. 6(a) or 6(b) form an instance of the shifted diffraction pattern that would be observed if the light would only leak in a particular direction. In both instances, only one of the first-order shifted diffraction spots can be collected by the objective lens. This is because, as it is shown in Figs. 6(a) and 6(b), the zero-order shifted diffraction spot and three of the four first-order shifted diffraction spots are outside of the numerical aperture of the objective lens. The portions of rings observed in the FP image are formed by the simultaneous rotation of the five vectors.[14] For any leaking direction at most, a diffraction spot is collected by the objective lens; therefore, the corresponding RP image would show a uniform intensity distribution because the Fourier transform of a shifted spot is proportional to an exponential function with an imaginary exponent.[4] The incoherent superposition of multiple uniform intensity distributions is a uniform intensity distribution; as such, the structure of the photonic crystal cannot be observed in the RP image corresponding to the FP image shown in Figs. 3(c) and 5(a). Nevertheless, as it was discussed above (Fig. 5), the structure of the plasmonic crystal can be recovered from the FP image using the FPIM technique. This is because the information about the photonic crystal structure is contained in the portion of rings observed in the FP image; i.e., in the trajectory described in the FP image by the only shifted diffraction spot collected by the objective lens when the direction of propagation of the surface waves changes. In the microscope's RP, the information about the position of the shifted diffraction spot is contained in the imaginary exponent of an exponential function; i.e., in the phase of the optical disturbance at the microscope's RP.[4,14] Therefore, all the information about the position of the shifted diffraction spot is lost in the RP image because the CCD camera is an intensity detector. This is the reason why the FP images shown in Figs. 2(e) and 2(g) contain more information about the photonic crystals than the RP images shown in Figs. 2(f) and 2(h), respectively.

It is worth noting that, in contrast with traditional microscopy techniques that use bulky optical condensers; in FPIM, it is not necessary that the zero-order diffraction ring be collected by the microscope objective lens. This has an important implication for the resolution achievable using the FPIM technique. The best resolution obtainable using a traditional microscope condenser is given by Eq. (1) when $NA_c = NA_o$. As it is shown in Figs. 2(e)–2(h), when $NA_c > NA_o$ the objective lens cannot collect the zero-order diffraction ring; therefore, no trace of the plasmonic crystal structure can be observed in the RP image. However, as it is shown in Fig. 5, FPIM allows for the recovery of the plasmonic crystal image because FPIM can recover the zero-order diffraction ring from the portions of the first-order diffraction rings present in the FP image. Therefore, the resolution limit using FPIM is given by Eq. (1) without the restriction $NA_c \leq NA_o$. Consequently, FPIM has the potential for producing images with a resolution well below $\lambda/(2NA_o)$ when $NA_c \gg NA_o$.

V. MICROSCOPE-BASED SPECTROMETER

Further analysis using different band-pass filters, revealed that the location of the diffraction features in the FP images, with the $NA_c = 0.28$ bulky condenser rings observed in the FP image shown in Figure 3(b), the spots corresponding to perpendicular illumination, or the thin $NA_c = 1.4$ condenser-like rings, for a given PC period are all frequency dependent. As such, a natural application of our microscope arrangement is spectrometry. Figs. 7(a) and 7(b) show the FP images obtained when illuminating the PC comprised of air holes in a PMMA layer, seen schematically in Fig. 1(b), with the un-filtered white light illumination source with normal incidence and with a traditional bulky condenser, respectively. The absence of a filter reveals the spectrum of the white light in both instances and demonstrates that the PCs, when coupled with an oil immersion objective lens and a FP CCD camera, mimic the functions of a spectrometer. For small periods, the thin, large radius, condenser-like rings can also be used for spectrometry. Figures 7(c), 7(d), and 7(e) show how the location of the condenser-like rings vary when different $\Delta\lambda = 10$ nm band-pass filters, centered at $\lambda = 500$ nm, $\lambda = 570$ nm, and $\lambda = 633$ nm, respectively, are used, while imaging a PCs with period p = 250 nm. The first-order diffraction features corresponding to perpendicular illumination (spots) and the traditional condenser (rings) cannot be captured by the objective lens for this PC. Using a Nikon Digital Sight DS-Fi1 camera to image the FP, and taking images with a 2560 × 1920 resolution, our spectrometry arrangement can achieve a spectral resolution value of ~0.45 nm per FP camera pixel. It should be noted then that a

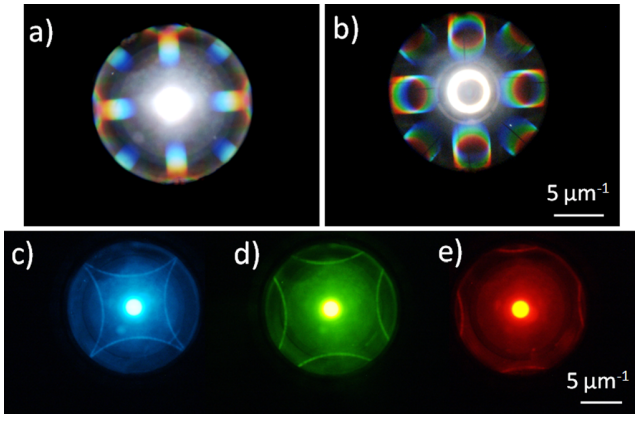

FIG. 7. (a) and (b) FP images of a photonic crystal with period $p = 600$ nm using white-light illumination and (a) a condenser and (b) no condenser. (c)–(e) FP images of the large condenser-like rings from a photonic crystal with period $p = 250$ nm, illuminated by a white-light source with different band-pass filters (c) 500 nm, (d) 570 nm, and (e) 633 nm applied.

simple PC with a subwavelength period can be used to transform an optical microscope prepared to implement the FPIM technique into a double feature instrument. For instance, a combination of a PC, a high *NA* objective lens, and a CCD constitute a compact instrument capable of producing high-resolution images, while simultaneously analyze the spectral composition of the light used for imaging.

VI. CONCLUSIONS

Adding an additional camera to a traditional compound microscope reveals the often overlooked, yet undoubtedly useful, microscope's Fourier Plane. The newly discovered condenser-like rings present in the FP images obtained with a perpendicular illumination source can be employed to reconstruct high-resolution RP images of photonic structures using the Fourier Plane Imaging Microscopy technique. Our ability to do so unequivocally demonstrates that the FP images obtained in this manner contain more information about the photonic crystals than the images recorded by the RP camera. We argue that our experimental results support the hypothesis that surface waves were optically excited in the studied photonic crystals thereby yielding both increased resolution and a novel approach to spectrometry. Further studies concerning the mechanism responsible for the excitation of surface waves using perpendicular illumination are currently in progress.

ACKNOWLEDGMENTS

This work was partially supported by the NSF CAREER Award (ECCS-0954490).

[1]P. Livingstone, *Still in Focus After all These Years* (R&D Magazine, 2011), Vol. 53, pp. 8–10.
[2]E. Hetcht, *Optics*, 3rd ed. (Addison Wesley, 1998).
[3]M. Born and E. Wolf, *Principles of Optics*, 5th ed. (Pergamon Press, 1975).
[4]J. W. Goodman, *Introduction to Fourier Optics* (McGraw-Hill, 1968).
[5]A. Vainrub, O. Pustovyy, and V. Vodyanoy, "Resolution of 90 nm (λ/5) in an optical transmission microscope with annular condenser," Opt. Lett. **31**, 2855–2857 (2006).
[6]S. Durant, Z. Liu, J. M. Steele, and X. Zhang, "Theory of the transmission properties of an optical far-field superlens for imaging beyond the diffraction limit," J. Opt. Soc. Am. B **23**(11), 2383–2392 (2006).
[7]H. H. Hopkins and P. M. Barham, "The influence of the condenser on microscopic resolution," Proc. Phys. Soc. **63**, 737–744 (1950).
[8]H. Köheler, "On Abbe's theory of image formation in the microscope," Opt. Acta **28**, 1691–1701 (1981).
[9]D. B. Desai, D. Dominguez, A. A. Bernussi, and L. Grave de Peralta, "Ultra-thin condensers for optical subwavelength resolution microscopy," J. Appl. Phys. **115**, 093103 (2014).
[10]G. Zheng, C. Kolner, and C. Yang, "Microscopy refocusing and dark-field imaging by using a simple LED array," Opt. Lett. **36**, 3987 (2011).
[11]G. Zheng, R. Horstmeyer, and C. Yang, "Wide-field, high-resolution Fourier ptychographic microscopy," Nature Photon. **7**, 739–745 (2013).
[12]D. Dominguez, L. Molina, D. B. Desai, T. O'Loughlin, A. A. Bernussi, and L. Grave de Peralta, "Hemispherical digital optical condensers with no lenses, mirrors, or moving parts," Opt. Express **22**, 6948–6957 (2014).
[13]J. D. Joannopoulos, S. G. Johnson, J. N. Winn, and R. D. Meade, *Photonic Crystals: Molding the Flow of Light* (Princeton University Press, 2008).
[14]R. Lopez-Boada, C. J. Regan, D. Dominguez, A. A. Bernussi, and L. Grave de Peralta, "Fundaments of optical far-field subwavelength resolution based on illumination with surface waves," Opt. Express **21**, 11928–11942 (2013).
[15]C. Kittel, *Introduction to Solid State Physics*, 7th ed. (John Wiley & Sons, 1996).
[16]L. C. Martin, *The Theory of the Microscope* (American Elsevier, 1966).
[17]S. P. Frisbie, C. F. Chesnutt, M. E. Holtz, A. Krishnan, L. Grave de Peralta, and A. A. Bernussi, "Image formation in wide-field microscopes based on leakage of surface plasmon-coupled fluorescence," IEEE Photon. J. **1**, 153 (2009).